Comparison of UAV-based digital elevation model with multi beam bathymetry for shallow water

Tuğba Kılıç *1 , **Onur Akyol** 2 , **Reha Metin Alkan** 1

1 Istanbul Technical University, Geomatics Engineering Department, Türkiye, tugba.kilic@itu.edu.tr, alkanr@itu.edu.tr
2 TUBITAK Marmara Research Center, Climate Change and Sustainability Vice Presidency, Marine Research and Technologies Research Group, Türkiye, onur.akyol@tubitak.gov.tr

Abstract

Accurate bathymetric data is essential for marine and coastal applications, particularly in shallow water regions. Unmanned Aerial Vehicle (UAV)-based systems are recognized for their cost-effectiveness and flexibility, making them a promising alternative in shallow-water environments where Multi Beam Echosounder (MBES) systems often face limitations due to high operational costs or logistical challenges. However, the UAV-based method is influenced by refraction effects, which result in underwater objects being perceived as shallower than their actual depth, leading to a decrease in the accuracy of the bathymetric model. To address this issue, the underestimation of water depth in submerged areas caused by refraction was evaluated using a correction algorithm. This study aims to assess the accuracy and usability of the UAV-based Digital Elevation Model (DEM) for seafloor mapping. For this assessment, the UAV-based DEM from the water body was compared with high-resolution three-dimensional (3D) seafloor topography obtained from a multi beam acoustic survey conducted in the same water area. The results indicated that an accuracy of 1.2 meters (RMSE) can be achieved in relatively shallow water areas up to a depth of 5 meters, while an accuracy of 2.0 meters (RMSE) is achievable at depths of around 15 meters. The study also highlighted the direct correlation between UAV-based DEM accuracy and depth, as well as the impact of sun glint on measurement accuracy. These findings underscore the potential of UAV technology to enhance bathymetric surveying capabilities, particularly in regions where MBES is either impractical or cost-prohibitive, thereby offering a valuable tool for comprehensive mapping and coastal studies.

1. Introduction

Bathymetric surveys are crucial for the accurate generation of 3D seafloor models, which are essential for a wide range of marine and coastal applications, including navigation, marine applications, morphological analysis, maritime spatial planning, and coastal engineering. Although various methods exist for generating 3D sea bottom models, acoustic techniques have become the standard tool for depth measurement today. The most commonly used acoustic depth measurement method is the single beam surveying technique, which is widely employed in numerous studies [1-2]. Generally recognized as the most traditional and low-risk form of seafloor data collection,

Single Beam Echosounder (SBES) technology provides relatively inexpensive and practical depth measurements. However, SBES is not designed for complete and continuous seafloor coverage, leaving gaps between survey lines. Depth measurements with multi beam systems, which eliminate this disadvantage by providing 100% coverage and are faster, have become widespread. Nevertheless, Multi Beam Echosounder (MBES) systems present operational and logistical challenges, typically requiring greater financial, technical, and labor resources for both operation and data analysis. In addition to all these, new surveying methods have emerged in the last few decades by changing bathymetric surveying platforms, and a paradigm shift has occurred in depth surveying. In this

context, Airborne Light Detection and Ranging (LiDAR), Satellite-Derived Bathymetry (SDB) and methods using Unmanned Aerial Vehicles (UAVs) are prominent. Airborne LiDAR enables the simultaneous and seamless acquisition of topographical LiDAR data for land and bathymetric measurements in neighboring ocean areas, offering substantial benefits. Although airborne LiDAR has the capability to measure depths in deep and turbid water conditions, the loss of laser energy caused by refraction, scattering, and absorption weakens the bottom return signal and restricts the maximum detectable depth. Airborne LiDAR instruments for bathymetric surveying can penetrate approximately three times the Secchi depth [3], corresponding to less than 100 meters in seawater under optimal conditions; therefore, this method is limited to shallow coastal areas [4]. Moreover, the significant costs associated with undertaking LiDAR surveys, primarily due to the considerable logistical efforts required to deploy a piloted airplane, place this approach beyond the scope of most projects.

In recent times, Satellite-Derived Bathymetry (SDB) has emerged as a rapid and cost-effective method for determining shallow-water bathymetry using satellite sensors. The widespread availability of no-cost, globally accessible nearshore satellite images makes it an attractive alternative. However, the challenge of SDB lies in the complex association of physical factors that influence the measured radiance, primarily the water's optical properties, the reflectance of the seabed, and depth [5].

Digital photogrammetry is advancing rapidly, propelled by innovations in camera technology, software, and algorithms for data extraction and processing [6]. The advent of UAV-based photogrammetry has proven to be an efficient alternative to traditional remote sensing techniques, offering significant improvements in spatial data acquisition capabilities. Compared to other remote sensing techniques, UAVs provide a cost-effective and flexible solution, with the advantage of delivering centimeter-scale spatial resolution and enabling surface data collection even under cloud cover. Furthermore, their ability to be equipped with a wide range of lightweight sensors makes them highly adaptable to diverse research objectives and user requirements. On the other hand, although UAVs have been used for many land surveys such as precision agriculture [7-8], forestry [9-10], architecture, engineering and construction [11-12], disaster management [13-14], it is seen in the literature that its use in bathymetric surveys is very limited. To summarize some of the studies in the literature, Woodget et al. [15] used the model developed by Westaway et al. [16]. In this study, Snell's Law was applied to the Digital Elevation Model (DEM), multiplying the apparent water depths by 1.34, the refractive index of clear water, to account for refraction effects. This correction assumes that the incidence and refraction angles are less than 10°. The resulting errors were between 0.05 and 0.08 meters, with average water depths ranging from 0.14 to 0.18 meters and maximum water depths of 0.50 and 0.70 meters. In a similar context, Chirayath and Li [17] proposed that, for a flat sea

surface and a nadir camera perspective, the perceived depth is generally about three-quarters of the true depth on Earth. Dietrich [18] extracted fluvial bathymetric data from unmanned aerial system imagery using Structure from Motion (SfM) and introduced a refraction correction method tailored for off-nadir SfM datasets using multicamera. Skarlatos and Agrafiotis [19] introduced an iterative simplified algorithm for correcting water refraction within the existing photogrammetric pipeline. In this correction model, a provisional Digital Surface Model (DSM) was utilized to iteratively adjust for refraction effects in the images. Initially, a provisional but erroneous DSM was computed, after which the images were corrected for refraction, and a new DSM was generated using the temporarily corrected imagery. The solution typically converged after three to four iterations. The performance of the proposed algorithm was assessed using LiDAR data. Their results indicate that, despite significant assumptions and approximations in the bundle adjustment and wave effects, the proposed algorithm was able to reduce the refraction effect to two times the ground pixel size. Partama et al. [20] introduced an innovative approach using co-registered image sequences or video frames to minimize the impact of water-surface reflections in UAV-based photogrammetry. When applied to a river section with depths up to 2.5 meters, this technique achieved accuracies between 5 and 15 cm, effectively clarified the reflected signals from the riverbed, and reduced the interference of moving light patterns.

As can be seen, there are only a limited number of studies on UAV-based bathymetric surveying; moreover, these studies are typically conducted in very shallow waters (i.e., a few decimeters to meters). In this study, unlike the previously mentioned studies in the literature, the usability and accuracy performance of UAV systems in bathymetric surveys were analyzed by comparing UAV measurements taken along a coastline with depths of around 15 meters to high accuracy multi beam acoustic surveying conducted in the same region. Detailed descriptions of the survey procedures and the resulting findings are provided in the following sections.

2. Method

A realistic test was conducted to assess the performance of UAV-based DEM for bathymetric surveying. In this context, a UAV survey was performed over a bay, encompassing the water body and the surrounding coastline. High accurate multi beam acoustic depth measurements were also conducted in the same area, providing an accurate reference 3D sea bottom topography. The bathymetric model obtained from the multi beam survey was then compared with the DEM generated by the UAV. Figure 1 illustrates the overall workflow of the study.
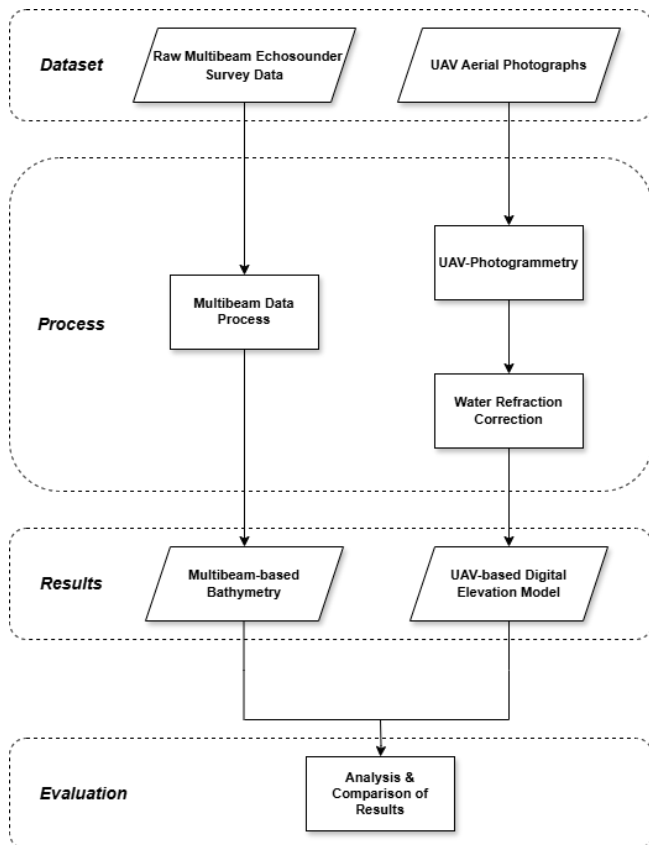
Figure 1. General workflow of the study

2.1. Empirical refraction correction

Photogrammetric techniques used in bathymetry must consider various external environmental and water-related factors, including weather conditions, luminosity, refraction, and water turbidity. These factors can influence the quality of aerial imagery and UAV performance, contributing to variations in the error margins of bathymetric representations for specific aquatic surfaces. Among these, water turbidity is particularly restricting, as the degree of turbidity determines the level of detail that can be captured for underwater features. Increased turbidity reduces both the quantity and quality of light in the water column [21]. Therefore, water should not be turbid enough to ensure a clear view of the bottom.

On the other hand, in through-water photogrammetry, the effect of light refraction at the air-water interface must be considered. Water introduces a two-media problem, disrupting the relationship that underpins the collinearity equations, which are used to calculate object coordinates from corresponding image coordinates [22]. Three essential factors must be considered when applying refraction correction: water refractive index, water surface elevation, and surface normal orientation. The ideal scenario assumes a flat-water surface, consistent water quality, and a constant refractive index [23].

The geometry of light refraction is described by Snell's Law as given in Eq. (1):

$$\frac{sinr}{sini} = \frac{h_R}{h_A} = \frac{n_1}{n_2} \tag{1}$$

where, r represents the angle of the refracted light ray above the water surface; i is the angle of the incident light ray coming from below the water surface; h_R denotes the true water depth; and h_A corresponds to the apparent water depth. The refractive index of air, n_2, equals 1, and n_1 is the refractive index of water. For clear water, the refractive index n_1 is defined as 1.34, with variations of less than 1% (±0.007) observed across a wide range of temperature and salinity conditions [24].

Without applying correction, the refraction issue between the two media leads to overestimating the actual bed depth or underestimating the water depth. The refraction correction method developed by Partama et al. [25] is based on the following Eq. (2):

$$h_R = \rho \cdot h_A \tag{2}$$

where, ρ is the correction factor of the model; h_R and h_A are the real and apparent depth calculated using the following Eq. (3) and Eq. (4):

$$\hat{h}_R \equiv \hat{z}_{sfc} - z_{R,btm} \tag{3}$$

$$\hat{h}_A \equiv \hat{z}_{sfc} - \hat{z}_{A,btm} \tag{4}$$

here, $\hat{z}_{sfc}$ is the water-surface; $z_{R,btm}$ is the real water bottom height measured by multi beam echosounder; and $\hat{z}_{A,btm}$ is the estimated apparent water bottom from photogrammetric reconstruction. If defined the biases (mean errors) in $\hat{h}_R$ and $\hat{h}_A$ as $\bar{\varepsilon}_R$ and $\bar{\varepsilon}_A$, respectively, Eq. (2) can be rewritten as:

$$\hat{h}_R = \rho \cdot \hat{h}_A + \beta \tag{5}$$

where, $\beta \equiv \rho \cdot \bar{\varepsilon}_A - \bar{\varepsilon}_R$ is the correction formula for water surface refraction [25].

2.2. Study area

The study area is defined as Ali Bostan Bay in Izmir, Türkiye. Situated along the Aegean Sea coast, Ali Bostan Bay is a natural bay known for its clear waters, making it an ideal site for research studies. The Bay's entrance is approximately 2.4 km wide, and it covers a surface area of about 327 hectares, with depths ranging from 1 to 30 meters. Weather conditions were stable for the season, with moderate wind speeds and low wave heights, which contributed to favorable measurement conditions. No significant negative factors were encountered, and the measurements were successfully completed. The site was selected to encompass both the shallowest point where bathymetric data could be collected and the deepest limit where DEM data could be obtained from the UAV, as represented by the red line in Figure 2.

Figure 2. Study area

2.3. Data collection

2.3.1. Bathymetric surveying with unmanned aerial vehicle

The successful completion of any photogrammetric project depends on thorough planning, which must be conducted before the work commences [26]. In this study, detailed planning was carried out prior to the project's initiation to ensure efficient execution, allowing for optimal outcomes and minimizing potential challenges. Aerial images were acquired using DJI Phantom 4 RTK (SZ DJI Technology Co., Ltd., China) quadcopter on 16 May 2022 under favorable weather and light conditions to ensure optimal data collection. The survey was conducted between 10:00 and 15:00, utilizing efficient flight planning to comprehensively cover the target area. The camera was programmed to automatically capture photos at each waypoint along a predetermined flight path, which was specifically designed to cover both ground and water areas, thereby ensuring the production of seamless data. Under clear skies and non flat-water surfaces, specular reflection of incident radiation creates bright white "sun glint" that obscures remotely sensed data, and this issue is particularly problematic in conditions where remote sensing would otherwise be most effective, such as in shallow waters, clear skies, and high-resolution imaging [27]. The most straightforward approach to minimizing sun glint is careful UAV flight time and direction planning. Nevertheless, due to the often uneven nature of the water surface, completely eliminating sun glint remains challenging [28]. To minimize the sun glint effect on the water surface, the camera was positioned at the nadir. The aerial survey was conducted over an area of 292.7 hectares, with a total flight duration of 80 minutes, resulting in 2,080 images. The overlapping rate for image matching in the SfM process was 80% for forward lap and 70% for side lap. These parameters have been selected to achieve accurate and efficient image processing. Table 1 provides an overview of the main UAV specifications used in this study.

Table 1. The main specifications of the UAV system used in this study [29]

Parameter	Value
Sensors	1'' CMOS, Effective Pixel: 20 M
Lens	FOV 84°, 8.8 mm/24 mm, f/2.8 - f/11, auto focus at 1 m - ∞
Takeoff Weight	1391 g
Maximum Flight Time	~30 minutes
Operating Temperature Range	0° to 40℃
GNSS Horizontal and Vertical Positioning Accuracy	H: 1 cm + 1 ppm (RMS) V: 1.5 cm + 1 ppm (RMS)

Direct georeferencing is an alternative technique for accurately reconstructing models within a specified reference system, thereby eliminating the requirement for Ground Control Points (GCPs). Using on-board Global Navigation Satellite System (GNSS) receivers in either single baseline Real Time Kinematic (RTK) or Network Real Time Kinematic (NRTK) mode enables the accurate recording of the UAV's position during each image capture. The UAV system used in this study, Phantom 4 RTK, includes an RTK GNSS module that provides accurate real-time data on camera positions. TUSAGA-Aktif as Türkiye's NRTK positioning system, which is being carried out within the scope of The Scientific and Technological Research Council of Türkiye (TUBITAK) supported R&D project and was completed in 2009, is operated under the joint ownership of the General Directorate of Land Registry and Cadastre (TKGM) and the Directorate General for Mapping (HGM) [30]. Similar to RTK Continuously Operating Reference Station (CORS) networks globally, the TUSAGA-Aktif network allows users to rapidly and cost-effectively determine position with a few centimeters-level accuracy in just minutes or even seconds.

2.3.2. Bathymetric surveying with multi beam echosounder

The bathymetric survey was conducted on 13 May 2022, spanning from 09:00 to 21:00. This survey covered an area of approximately 320 hectares using a small boat equipped with Multi Beam Echosounder (MBES) and other necessary measurement instruments. The use of the small boat was an ideal solution, as its smaller dimensions and the draft not only made the installation of the MBES components easier but also allowed for the measurement of shallower areas. MBES data were collected using the high-resolution, professional-level WASSP WMB-3250 multi beam echosounder (WASSP Ltd., New Zealand). Accurate spatial referencing of all MBES sensors is crucial for collecting high-quality data. Consequently, the MBES system was installed and set up following the manufacturer's guidelines and compliance with international standards. Table 2 provides an overview of the main MBES specifications used in this study.

Table 2. The main specifications of the MBES used in this study [31]

| Parameter	Value
Frequency	160 kHz
Beam Width	224 beams equidistant spacing over 120° port/starboard swath
Depth Range	2 - 200 m
Depth Resolution	7.5 cm
Operating Temperature	0° C to 40° C

2.4. Data processing

2.4.1. Unmanned aerial vehicle data processing

The reconstruction of 3D shapes from images has been significant over the past centuries [32]. SfM is a photogrammetric method used to generate a 3D point cloud from overlapping two-dimensional (2D) images, starting with the detection of features, which involves identifying distinctive elements in the images and matching these key points across them to establish correspondences [33]. SfM utilizes bundle adjustment algorithms with geometrically correct feature correspondences to simultaneously determine the 3D structure of a scene, the different camera poses (extrinsic calibration), and the camera's intrinsic parameters (intrinsic calibration). After bundle adjustment, a Multi-View Stereo (MVS) algorithm is applied to generate extra points and create a dense point cloud. At this stage, the point density increases, resulting in a more accurate surface representation than sparse point clouds [34]. The entire process is known as SfM-MVS.

The image processing began with SfM, which was used to estimate the camera's extrinsic and intrinsic parameters, as well as to determine the spatial coordinates of a sparse point cloud. Following this, MVS was utilized to densify the point cloud, resulting in a high-resolution dense point cloud that more accurately captured surface details. Based on this, DEM and orthophoto were generated to represent the terrain and surface textures. The spatial resolution of the orthophoto was 4 cm, providing detailed and high-resolution data for subsequent analysis. DEM was initially generated with ellipsoidal heights reflecting the depth relative to a predefined reference ellipsoid, featuring a spatial resolution of 9 cm to ensure high-detail representation.

Sea level monitoring in Türkiye, managed by the Directorate General for Mapping (HGM) through the Turkish National Sea Level Monitoring System (TUDES), employs 20 GNSS-integrated radar sensor tide gauge stations adhering to GLOSS standards, which record sea level measurements every 15 minutes and monitor meteorological parameters like atmospheric pressure, wind speed, and temperature affecting sea level changes [35]. DEM was converted from ellipsoidal to orthometric heights, aligning it to a geoid-based vertical reference. This transformation utilized the known height difference between ellipsoidal and orthometric values at the Menteş tide gauge station (38°26' N, 26°43' E), part of the TUDES network. This processing step aligns the DEM and bathymetry data to the same vertical datum, ensuring the integration of

datasets for accurate spatial comparisons and analyses. The generated DEM is presented in Figure 3.
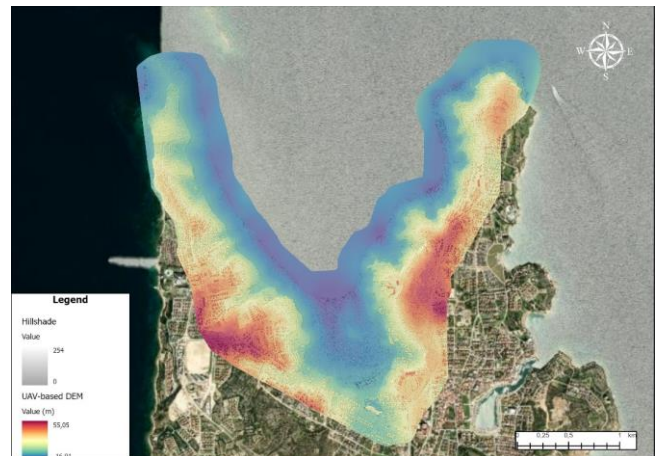

Figure 3. UAV-based DEM map

To use refraction correction algorithms, a water surface model should be constructed by extracting water edges from the resulting orthophoto and DEM [36]. For this purpose, water edge points were determined throughout the study area, and an estimated water surface model was produced. As can be seen from Eq. (3) and Eq. (4), the vertical distance between the water surface and the sea bottom was defined as depth. The refraction-induced overestimation of seabed depth in submerged areas was assessed using a correction algorithm. This correction was applied using Eq. (5) to raw UAV-based DEM depths. In this study, the values $\rho = 1.34$ and $\beta = 0$, as proposed by Westaway et al. [16], were used. All results presented hereafter pertain to the UAV-based DEM with refraction correction.

2.4.2. Multi beam echosounder data processing

Bathymetric data processing involves the transformation of raw depth measurements obtained from bathymetric surveys into usable and visually interpretable information about the underwater topography. Bathymetric measurement uncertainties are influenced by various factors, including the transducer's draft setting, spatial and temporal variations in sound velocity, motion (heave, pitch, and roll effects), the vessel's settlement and squat in the water, and errors in tidal corrections. Additionally, the GNSS positioning system is affected by various error sources, such as satellite clock and orbital errors, receiver clock errors, tropospheric and ionospheric delays, antenna phase center offsets and variations, as well as integer ambiguities and phase delays in carrier phase measurements. To accurately obtain the seafloor, multi beam measurements must be aligned with the true vertical as indicated by the motion sensor and the heading reported by the gyro compass. In summary, the overall accuracy largely depends on the integration of sensors that measure horizontal and vertical positioning, orientation, and sound speed. The simplest alignment method, known as the "Patch Test," is a calibration procedure conducted aboard the research vessel during the initial installation of the equipment. It is a data measurement method used to calculate the sonar head's

offset angle while minimizing bathymetric errors by comparing two datasets from a certain seabed area [37]. A complete patch test was conducted in the study area, and offsets were applied to ensure accurate positioning. Another step involves correcting the beam vector's refracted path through the ocean's varying sound speed structure, which is influenced by changes in temperature and salinity driven by oceanographic factors. Measurements were conducted aboard the vessel using a Valeport SWiFT SVP (Teledyne Valeport Ltd., UK) to obtain a vertical profile of the sound speed. Additionally, the Menteş tide gauge station was the reference point for accurately determining sea level. After completing these mentioned procedures, the bathymetric model was generated (Figure 4).
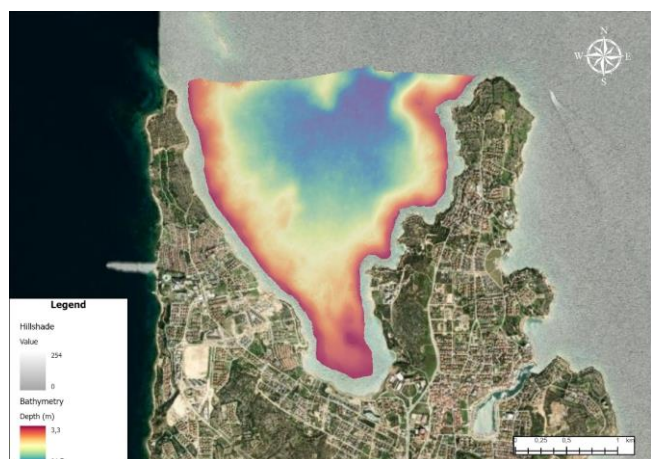
Figure 4. Seafloor topography produced with multi beam surveying

Bathymetric points were transferred to Fledermaus (Quality Positioning Services BV, The Netherlands) software to enhance the visualization and interpretation of underwater data. Fledermaus is purpose-built for the exploration and analysis of multi beam bathymetric data, allowing users to visualize and enhance the data to create accurate bathymetric plots. The multi beam data was visualized in 3D using Fledermaus, and subsequent data analysis was conducted to interpret and extract relevant information from the visualized data.

3. Results and Discussion

The results were compared with multi beam bathymetry after applying the correction factor to UAV-based DEM. For comparison, $1\,m\,x\,1\,m$ grid was created with the same resolution as the multi beam bathymetry, and depth information was extracted from both data sets for each point on the grid. As shown in Figure 5, no sun glint effect was observed in the western part of the study area (regions a and b), whereas noticeable sun glint effects were present in the northeastern part (regions c and d).


Figure 5. Examples of specific regions in the orthophoto

It was revealed that the points where the relationship between the UAV-based DEM and the multi beam bathymetry deviated the most were located in the northeastern part of the study area and were directly related to depth (Figures 6 and 7). Due to the sun glint effect mentioned, the deviation of DEM compared to bathymetry data in this region was an expected result of the study.
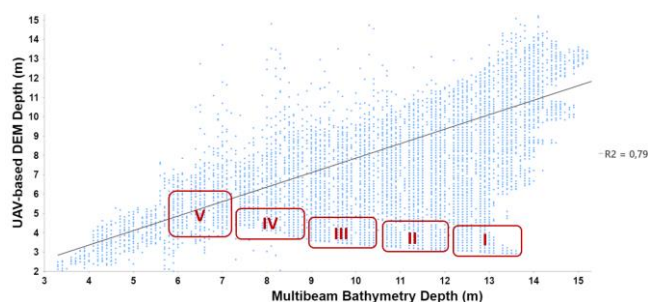
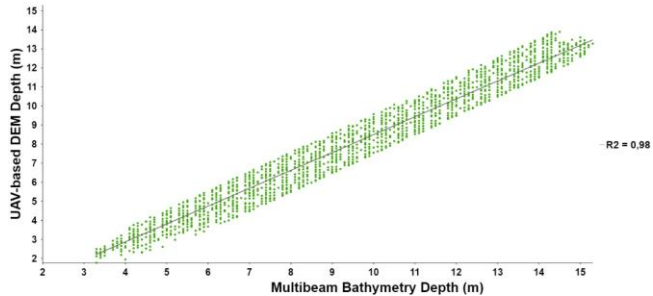**Figure 6.** Relationship between multi beam bathymetry and UAV-based DEM
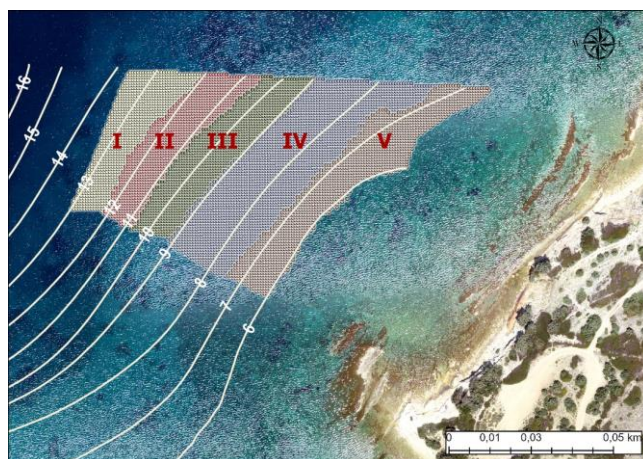
Figure 7. Distribution of labelled points on orthophoto

Outliers were detected and removed from the dataset to eliminate disturbances. Table 3 summarizes the statistical properties of the datasets, and Figure 8 illustrates their relationship.

Table 3. Statistics for multi beam bathymetry and UAV-based DEM

Data	Min. (m)	Max. (m)	Mean (m)	Std. Dev. (m)
Multi Beam Bathymetry	3.30	15.30	8.12	2.23
UAV-based DEM	1.77	13.91	6.73	2.11

Figure 8. Relationship between multi beam bathymetry and UAV-based DEM after outlier removal

The depth differences between the multi beam bathymetry and UAV-based DEM at each grid point have been calculated. This approach ensures a detailed assessment of the variations between the two datasets, providing a spatial representation of their differences. Figure 9 illustrates the distribution of differences.
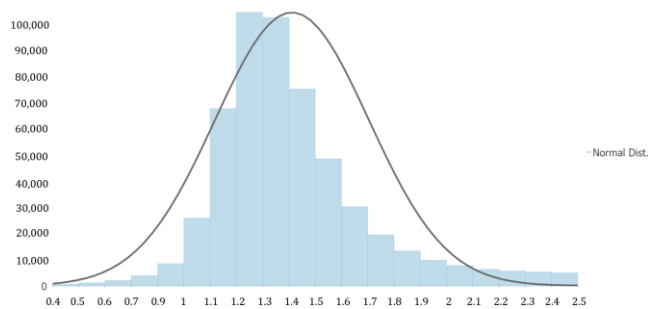
Figure 9. Distribution of differences between multi beam bathymetry and UAV-based DEM

Depths were categorized into four classes to assess the relationship between the datasets: 3.30–5.00 m, 5.10–10.00 m, 10.10–15.00 m, and 15.10–15.30 m. The differences were analyzed within each depth class. Key statistical metrics, including the minimum, maximum, mean, standard deviation, and Root Mean Square Error (RMSE), were calculated and are summarized in Table 4.

Table 4. Statistics for differences between multi beam bathymetry and UAV-based DEM

Classes	Depth Ranges (m)	Min. (m)	Max. (m)	Mean (m)	Std. Dev. (m)	RMSE (m)
Class 1	3.30 - 5.00	0.43	2.29	1.16	0.14	1.17
Class 2	5.10 - 10.00	0.43	2.54	1.34	0.26	1.37
Class 3	10.10 - 15.00	0.44	2.54	1.59	0.37	1.64
Class 4	15.10 - 15.30	1.61	2.39	1.99	0.17	2.00

For the shallowest depth class, the minimum and maximum differences were 0.43 m and 2.29 m, respectively, with a mean of 1.16 m. The standard deviation was relatively low at 0.14 m, indicating consistency in the measurements within this class. The RMSE for this class was 1.17 m, which reflects the minimum level of error in the depth estimations. For the following class, mean depth differences were 1.34 m. This class exhibited a slightly higher standard deviation, 0.26 m, compared to class 1, suggesting a slightly greater variability in the measurements. The RMSE of 1.37 m indicates a modest increase in UAV measurement error compared to Class 1. In class 3, the mean differences were 1.59 m. The standard deviation increased further to 0.37 m, and the RMSE was 1.64 m, reflecting a higher degree of variability and error in this deeper class. The final class, which covers the deepest range, had minimum and maximum depth differences of 1.61 m and 2.39 m, respectively, with a mean of 1.99 m. The standard deviation was relatively low, 0.17 m, and the RMSE increased to 2.00 m, indicating that the accuracy of UAV depth estimation in this range was slightly more prone to error.

The results demonstrate a trend of increasing variability and decreasing accuracy in the UAV-based DEM as depth increases. In shallower regions, the UAV-based DEM aligns well with the multi beam bathymetry, as reflected by lower mean differences, standard deviations, and RMSE values. This indicates that UAV-based systems perform effectively in shallow areas where environmental factors are less challenging. However, as depths increase, the discrepancies between the two datasets become more pronounced. Higher mean differences, larger variability, and greater RMSE values in deeper zones suggest a reduction in the accuracy and reliability of UAV-based DEM.

Figure 10. Spatial distribution of differences between multi beam bathymetry and UAV-based DEM

Figure 10 illustrates the spatial distribution of differences within the study area. Minimal differences are predominantly observed along the coastline, where the UAV-based DEM demonstrates strong alignment with the bathymetry data. Additionally, the central part of the bay, represented by predominantly green tones on the map, shows a high degree of correlation between the datasets. This alignment can be attributed to favourable environmental conditions during the UAV survey, such as low turbidity and high water clarity, which enhanced the accuracy of measurements in shallow waters. However, the figure also indicates an increase in discrepancies in regions farthest from the shoreline.

These differences can be attributed to various factors, including water surface conditions, turbidity, sun glint, and seafloor texture, all of which contribute to the complexities affecting data accuracy. Among these, refraction emerges as the dominant factor when it comes to shallow waters, significantly influencing both the geometric and radiometric properties of the data. This, in turn, impacts the outcomes of image-based 3D reconstruction methods. To mitigate these effects, the development of a refraction correction algorithm specifically tailored to the unique characteristics of the study area is crucial. Such an algorithm would address site-specific challenges, improving the accuracy of the data and the reliability of the comparative analysis between the datasets.

4. **Conclusion**

This study investigates the usability of Unmanned Aerial Vehicle (UAV)-based mapping systems for bathymetric measurements. For this purpose, 3D seafloor topography obtained from bathymetric measurements conducted in the same area using the multi beam system, one of the most accurate bathymetric surveying technologies available, was used as the reference surface. The UAV-based results were systematically compared against these reference measurements. Given that the comparisons covered an extensive area with points at varying depths, the findings are expected to be realistic and accurate. The analysis revealed a strong correlation between the accuracy of UAV-based measurements and depth, with accuracy decreasing in deeper waters. Additionally, the study emphasized the distorting effects of sun glint on the UAV-based Digital Elevation Model (DEM), which can introduce significant errors. Overall, the method demonstrated that, in relatively shallow water areas, an accuracy of 1.2 meters can be achieved at depths up to 5 meters and 2.0 meters at depths of approximately 15 meters.

Beyond bathymetric mapping, the UAV system also captured the surrounding landmass, enabling the creation of a topobathymetric surface, which provides a comprehensive view of both terrestrial and underwater topography. Additionally, one of the critical global challenges in bathymetric studies is the integration of echosounding data with UAV data to enhance accuracy, making this combined approach crucial for the comprehensive mapping of shallow-water coastal areas. Incorporating multiple data sources can substantially improve the accuracy and completeness of bathymetric maps. While multi beam surveys typically do not cover water depths shallower than 5 to 10 meters or are labor- and cost-intensive when they do, UAV-based DEMs can effectively survey these shallower depths.

Each technique examined in this study has unique advantages and limitations, making it more appropriate for specific applications. The comparison of the two methods highlights significant differences in terms of workforce, time, and cost efficiency. For instance, the UAV surveys required only two personnel to complete the measurements, whereas the MBES surveys involved a team of seven individuals, including engineers, captains, and crew members. This disparity in personnel requirements reflects the differing operational complexities of the two approaches. In terms of time, the UAV surveys were notably more efficient, taking just 5 hours to complete the data collection compared to the 12 hours required for the MBES surveys. This efficiency stems from the UAV's ability to rapidly cover the study area without the logistical challenges associated with vessel operations. When comparing the costs of the two methods, the UAV surveys proved to be significantly more economical. Considering realistic and feasible market conditions, the total cost of a UAV-based bathymetric measurement is approximately 5% of the cost of the MBES measurement. This substantial cost difference can be attributed to several factors, including reduced workforce requirements, shorter operational time, and lower equipment and software prices compared to MBES.

When considering these factors in UAV-based systems, this method emerges as a highly rapid, cost-effective, and straightforward approach. The method provides relatively accurate bathymetric measurements, especially in challenging environments such as coral reefs and rocky underwater terrains, where the deployment of multi beam or single beam systems is often highly difficult or unfeasible. It is particularly effective for estimating depth during presurvey evaluations or feasibility studies, providing reliable data that supports evidence-based decision-making. UAV-based bathymetric surveying is also valuable for coastal zone management and environmental monitoring, particularly in tracking shoreline erosion, sediment transport, and changes in coastal morphology. These bathymetric models contribute to sustainable development and strategies for mitigating coastal degradation. In disaster response scenarios, UAV technology enables rapid assessments of submerged infrastructure and seafloor alterations, significantly enhancing relief and recovery efforts. Additionally, the high-resolution bathymetric data generated by UAV systems facilitates supporting habitat mapping, detecting changes in marine ecosystems, and assessing the impacts of human activities on biodiversity. Despite these advantages, however, UAV-based methods have limited applicability in water bodies exceeding several tens of meters in depth due to factors such as water turbidity, wave conditions, and meteorological influences impacting accuracy. Consequently, while UAV-based bathymetric mapping systems cannot fully replace traditional methods, such as multi beam echosounders, they provide an efficient and cost-effective solution in scenarios where decimeter- or meter-level accuracy is acceptable. However, due to their superior accuracy and reliability, traditional methods remain the preferred choice for applications requiring sub-decimeter accuracy or surveys in deeper waters. Thus, UAV-based systems are best seen as complementary tools in the broader field of bathymetric surveying, offering flexibility and efficiency in specific contexts.

Acknowledgments

Author contributions

Tuğba Kılıç: Conceptualization, Methodology, Software, Visualization, Investigation, Writing-Original draft preparation, Field study, Writing-Reviewing and Editing **Onur Akyol:** Methodology, Software, Investigation, Field study **Reha Metin Alkan:** Conceptualization, Methodology, Investigation, Writing-Original draft preparation, Writing-Reviewing and Editing.

Conflicts of interest

The authors declare no conflicts of interest.

References

1. Snellen, M., Siemes, K., & Simons, D. G. (2011). Model-based sediment classification using single-beam echosounder signals. The Journal of the Acoustical Society of America, 129(5), 2878-2888.

2. Landero Figueroa, M. M., Parsons, M. J., Saunders, B. J., Radford, B., Salgado-Kent, C., & Parnum, I. M. (2021). The use of singlebeam echo-sounder depth data to produce demersal fish distribution models that are comparable to models produced using multibeam echo-sounder depth. Ecology and Evolution, 11(24), 17873-17884.

3. Peeri, S., Gardner, J. V., Ward, L. G., & Morrison, J. R. (2010). The seafloor: A key factor in LiDAR bottom detection. IEEE Transactions on Geoscience and Remote Sensing, 49(3), 1150-1157.

4. Hell, B. (2011). Mapping bathymetry: From measurement to applications. (Doctoral dissertation). Stockholm University, Department of Geological Sciences, Stockholm.

5. Kim, M., Danielson, J., Storlazzi, C., & Park, S. (2024). Physics-Based Satellite-Derived Bathymetry (SDB) Using Landsat OLI Images. Remote Sensing, 16(5), 843.

6. Serwa, A. (2016). Development of Software Application for Digital Photogrammetric Systems (ADPS): Basic Level. International Conference on Civil and Architecture Engineering, (pp. 1-15). Military Technical College, April 19-21.

7. Zhang, C., & Kovacs, J. M. (2012). The application of small unmanned aerial systems for precision agriculture: a review. Precision Agriculture, 13, 693-712.

8. Radoglou-Grammatikis, P., Sarigiannidis, P., Lagkas, T., & Moscholios, I. (2020). A compilation of UAV applications for precision agriculture. Computer Networks, 172, 107148.

9. Adão, T., Hruška, J., Pádua, L., Bessa, J., Peres, E., Morais, R., & Sousa, J. J. (2017). Hyperspectral imaging: A review on UAV-based sensors, data processing and applications for agriculture and forestry. Remote Sensing, 9(11), 1110.

10. Selim, S., Demir, N., & Şahin, S. O. (2022). Automatic detection of forest trees from digital surface models derived by aerial images. International Journal of Engineering and Geosciences, 7(3), 208-213.

11. Şasi, A., & Yakar, M. (2018). Photogrammetric modelling of Hasbey Dar'ülhuffaz (Masjid) using an unmanned aerial vehicle. International Journal of Engineering and Geosciences, 3(1), 6-11. https://doi.org/10.26833/ijeg.328919.

12. Kanun, E., Alptekin, A., & Yakar, M. (2021). Cultural heritage modelling using UAV photogrammetric methods: a case study of Kanlıdivane archeological site. Advanced UAV, 1(1), 24-33.

13. İlhan, S., & Aydar, U. (2023). Flood analysis of Çan (Kocabaş) stream with UAV images. Advanced UAV, 3(1), 25-34.

14. Ağca, M., Gültekin, N., & Kaya, E. (2020). İnsansız hava aracından elde edilen veriler ile kaya düşme potansiyelinin değerlendirilmesi: Adam Kayalar örneği, Mersin. Geomatik, 5(2), 134-145.

15. Woodget, A. S., Carbonneau, P. E., Visser, F., & Maddock, I. P. (2015). Quantifying submerged fluvial topography using hyperspatial resolution UAS imagery and structure from motion photogrammetry. Earth Surface Processes and Landforms, 40(1), 47-64.

16. Westaway, R. M., Lane, S. N., & Hicks, D. M. (2000). The development of an automated correction procedure for digital photogrammetry for the study of wide, shallow, gravel-bed rivers. Earth Surface Processes and Landforms: The Journal of the British Geomorphological Research Group, 25(2), 209-226.

17. Chirayath, V., & Li, A. (2019). Next-generation optical sensing technologies for exploring ocean worlds—NASA FluidCam, MiDAR, and NeMO-Net. Frontiers in Marine Science, 6, 521.

18. Dietrich, J. T. (2017). Bathymetric structure-from-motion: Extracting shallow stream bathymetry from multi-view stereo photogrammetry. Earth Surface Processes and Landforms, 42(2), 355-364.

19. Skarlatos, D., & Agrafiotis, P. (2018). A novel iterative water refraction correction algorithm for use in structure from motion photogrammetric pipeline. Journal of Marine Science and Engineering, 6(3), 77.

20. Partama, I. G. Y., Kanno, A., Ueda, M., Akamatsu, Y., Inui, R., Sekine, M., Yamamoto, K., Imai, T., & Higuchi, T. (2018). Removal of water-surface reflection effects with a temporal minimum filter for UAV-based shallow-water photogrammetry. Earth Surface Processes and Landforms, 43(12), 2673-2682.

21. Bussières, S., Kinnard, C., Clermont, M., Campeau, S., Dubé-Richard, D., Bordeleau, P. A., & Roy, A. (2022). Monitoring Water Turbidity in a Temperate Floodplain Using UAV: Potential and Challenges. Canadian Journal of Remote Sensing, 48(4), 565-574.

22. Westaway, R. M., Lane, S. N., & Hicks, D. M. (2001). Remote sensing of clear-water, shallow, gravel-bed rivers using digital photogrammetry. Photogrammetric Engineering and Remote Sensing, 67(11), 1271-1282.

23. Cao, B., Fang, Y., Jiang, Z., Gao, L., & Hu, H. (2019). Shallow water bathymetry from WorldView-2 stereo imagery using two-media photogrammetry. European Journal of Remote Sensing, 52(1), 506-521.

24. Jerlov, N. G. (1976). Marine optics. Elsevier.

25. Partama, I. G. Y., Kanno, A., Akamatsu, Y., Inui, R., Goto, M., & Sekine, M. (2017). A simple and empirical refraction correction method for UAV-based shallow-water photogrammetry. International Journal of Geological and Environmental Engineering, 11(4), 295-302.

26. Serwa, A., & El-Semary, H. H. (2016). Integration of soft computational simulator and strapdown inertial navigation system for aerial surveying project planning. Spatial Information Research, 24, 279-290.

27. Hedley, J. D., Harborne, A. R., & Mumby, P. J. (2005). Simple and robust removal of sun glint for mapping shallow-water benthos. International Journal of Remote Sensing, 26(10), 2107-2112.

28. Tiškus, E., Bučas, M., Vaičiūtė, D., Gintauskas, J., & Babrauskienė, I. (2023). An Evaluation of Sun-Glint Correction Methods for UAV-Derived Secchi Depth Estimations in Inland Water Bodies. Drones, 7(9), 546.

29. DJI (2024). Support Phantom 4 RTK, Specs.

30. General Directorate of Land Registry and Cadastre (2024). TUSAGA-Aktif System.

31. WASSP (2024). WMB-3250 Manuals.

32. Eltner, A., Kaiser, A., Castillo, C., Rock, G., Neugirg, F., & Abellán, A. (2016). Image-based surface reconstruction in geomorphometry–merits, limits and developments. Earth Surface Dynamics, 4(2), 359-389.

33. Meinen, B. U., & Robinson, D. T. (2020). Mapping erosion and deposition in an agricultural landscape: Optimization of UAV image acquisition schemes for SfM-MVS. Remote Sensing of Environment, 239, 111666.

34. Zeybek, M. (2021). Classification of UAV point clouds by random forest machine learning algorithm. Turkish Journal of Engineering, 5(2), 48-57.

35. TUDES (2024). Sea Level Observations.

36. Bagheri, O., Ghodsian, M., & Saadatseresht, M. (2015). Reach scale application of UAV+ SfM method in shallow rivers hyperspatial bathymetry. The International Archives of the Photogrammetry, Remote Sensing and Spatial Information Sciences, 40, 77-81.

37. Kim, H. D., Aoki, S. I., Kim, K. H., Kim, J., Shin, B. S., & Lee, K. (2020). Bathymetric survey for seabed topography using multibeam echo sounder in wando, korea. Journal of Coastal Research, 95(SI), 527-531.